View metadata, citation and similar papers at core.ac.uk
brought to you by CORE
provided by DSpace at Belgorod State University

ON X–RAY SOURCES BASED ON CHERENKOV AND QUASI-CHERENKOV EMISSION MECHANISMS

C. Gary[1], V. Kaplin[2], A. Kubankin[3], V. Likhachev[3], N. Nasonov[3], M. Piestrup[1], S. Uglov[2]

[1] *Adelphi Technology, Inc. 981-B Industrial Rd. San–Carlos, CA 94070, USA*

[2] *NPI Tomsk Polytechnic University, Lenin Ave. 2-A, Tomsk, 634050, Russia*

[3] *Laboratory of Radiation Physics, Belgorod State University, 14 Studencheskaya st., Belgorod, 308007, Russia*

Abstract A variety of possible schemes of X–ray sources based on Cherenkov like emission mechanisms is considered theoretically. The possibility to increase substantially an angular density of parametric X–ray source under conditions of grazing incidence of emitting relativistic electrons on the reflecting crystallographic plane of a crystalline target is shown. The growth of Cherenkov X–ray angular density due to modification of the structure of Cherenkov cone in conditions of grazing incidence of an electron beam in the surface of a target is discussed as well as the peculiarities of Cherenkov X–ray generation from relativistic electrons crossing a multilayer nanostructure. The question of relative contributions of parametric X–ray and diffracted bremsstrahlung to total emission yield from relativistic electrons moving in a perfect crystal is elucidated. X–ray generation during multipasses of an electron beam through an internal target in circular accelerator is considered as well.

Keywords: Relativistic electron, Cherenkov X–ray radiation, Parametric X–ray radiation, Bremsstrahlung, X–ray source

1. Introduction

Creation of an effective and inexpective X–ray source alternative to synchrotrons is a major focus of interest for the studies of coherent emission from relativistic electrons in dense media. A number of novel sources based on transition radiation [1], channelling radiation [2], parametric X–ray radiation [3], Cherenkov radiation [4] have been studied and considered as candidates for possible applications. However, the intensity

H. Wiedemann (ed.), Advanced Radiation Sources and Applications, 235–265.
© 2006 *Springer. Printed in the Netherlands.*

of these sources must be increased for them to be practical [5]. Because of this, the study of new possibilities to increase the spectral-angular density of such sources is a subject of much current interest.

The main attention in this paper is devoted to the analysis of Cherenkov like emission mechanisms. Substantial disadvantage of these mechanisms consists in the strongly non-uniform angular distribution of emitted photons close to a hollow cone. As a consequence one should collimate the emitted flux to obtain a uniform photon distribution on the surface of irradiated test specimen. A possibility to use the effect of emission cone modification in order to increase the part of collimated photon flux employed is studied in this paper. Parametric X–rays (PXR) from relativistic electrons moving in a crystal or multilayer nanostructure is considered in Sec.2. Substantial growth of PXR local angular density in conditions of small orientation angles of the emitting particle velocity relative to reflecting crystallographic plane is shown. Sec.3 is devoted to study of Cherenkov X–ray radiation in the vicinity of photoabsorption edge of the target's material [1, 6–20].The case of grazing incidence of emitting electrons on the surface of the target is the object of investigations.

Cherenkov X–ray radiation from relativistic electrons crossing a multilayer nanostructure is considered in Sec.4 of this paper. This scheme is of interest because of possible arrangement of the irradiated test specimen in the immediate vicinity of the multilayer due to large emission angles achievable on condition under consideration.

Relative contributions of PXR and diffracted bremsstrahlung to total emission yield from relativistic electrons crossing a perfect crystal are studied in Sec.5. This problem is of the great interest because the results of some recent experiments [11, 12] are in contradiction with the generally accepted opinion that PXR yield is determined in the main by the Bragg scattering of the fast particle Coulomb field (actually PXR emission mechanism). Performed studied show that the contribution of diffracted bremsstrahlung to total PXR yield may be very substantial in contrast with above opinion.

2. PXR in conditions of small orientation angles of emitting particle velocity relative to reflecting plane

Let us consider properties of PXR from relativistic electrons moving through a crystal aligned by reflecting crystallographic plane at the small angle $\varphi/2$ to the velocity of the emitting electron (see Fig.1). The well known kinematical formula for the spectral-angular distribution of

emitted PXR energy [3, 13]

$$\frac{\mathrm{d}E}{\mathrm{d}t\,\mathrm{d}\omega\,\mathrm{d}\Omega} = \frac{8\pi Z^2 e^6 n_a^2 |S(\mathbf{g})|^2 \mathrm{e}^{-g^2 u_T^2}}{m^2(1+g^2R^2)^2} \frac{(\epsilon\omega\mathbf{v}-\mathbf{g})^2 - [\epsilon\omega(\mathbf{n},\mathbf{v})-(\mathbf{n},\mathbf{g})]^2}{\left[g^2+2\omega\sqrt{\epsilon}(\mathbf{n},\mathbf{g})\right]^2} \times\delta\left[\omega\left(1-\sqrt{\epsilon}(\mathbf{n},\mathbf{v})\right)-(\mathbf{g},\mathbf{v})\right] \quad (1)$$

is used for our purposes. Here Z is the atomic number of the crystalline target, n_a is its atomic density, $S(\mathbf{g})$ is the structure factor of an elementary cell, $\mathbf{g}$ is the reciprocal lattice vector, $u_T$is the mean square amplitude of thermal vibrations of atoms, R is the screening radius in the Fermi-Thomas atom model, the simplest model with exponential screening is used, $\epsilon = 1-\omega_0^2/\omega^2$, ω_0 is the plasma frequency, $\mathbf{n}$ is the unit vector to the direction of emitted photon propagation, $\mathbf{v}$ is the velocity of emitting electron.

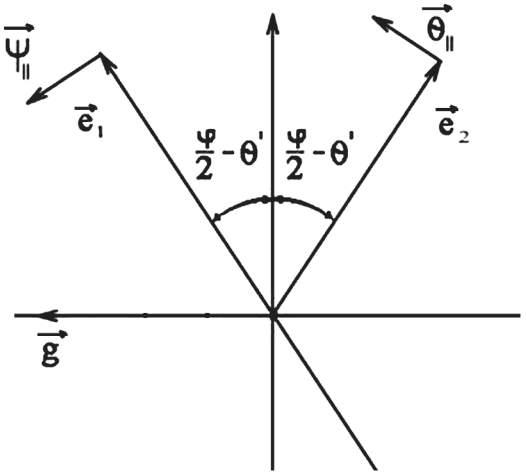

Figure 1. The geometry of PXR process. $\mathbf{e}_1$ is the axis of the emitting electron beam, $\mathbf{e}_2$ is the axis of the emitted photon flux, θ' is the orientation angle describing possible turning of the crystalline target by the goniometer, $\mathbf{g}$ is the reciprocal lattice vector, $\Theta_\parallel$ and $\Psi_\parallel$ are the components of the angular variables $\mathbf{\Theta}$ and $\mathbf{\Psi}$ parallel to the plane determined by the vectors $\mathbf{e}_1$ and $\mathbf{e}_2$.

Introducing the angular variables $\mathbf{\Theta}$ and $\mathbf{\Psi}$ in accordance with formulae

$$\begin{aligned} \mathbf{v} &= \mathbf{e}_1\left(1-\tfrac{1}{2}\gamma^{-2}-\tfrac{1}{2}\Psi^2\right)+\mathbf{\Psi}, \qquad (\mathbf{e}_1,\mathbf{\Psi})=0, \\ \mathbf{n} &= \mathbf{e}_2\left(1-\tfrac{1}{2}\Theta^2\right)+\mathbf{\Theta}, \qquad (\mathbf{e}_2,\mathbf{\Theta})=0, \qquad (\mathbf{e}_1,\mathbf{e}_2)=\cos\varphi, \quad (2) \end{aligned}$$

one can reduce the formula (1) to more simple form in the case of small orientational angle $\varphi/2 \ll 1$ under consideration

$$\frac{\mathrm{d}E}{\mathrm{d}t\,\mathrm{d}\omega\,\mathrm{d}^2\Theta} \approx E_0 \frac{g}{\omega} \frac{\frac{g}{\omega}(\frac{g}{\omega} - \varphi + 2\theta' + 2\Theta_\parallel) - \frac{1}{\gamma^2}}{(\frac{g}{\omega} - \varphi + 2\theta' + 2\Theta_\parallel)^2} \tag{3}$$
$$\times\, \delta\left[\frac{1}{\gamma^2} + (\Psi_\perp - \Theta_\perp)^2 + (\varphi + \Psi_\parallel - \Theta_\parallel)^2 - \frac{g}{\omega}(\varphi + 2\theta' + 2\Psi_\parallel)\right],$$
$$E_0 = \frac{16\pi Z^2 e^6 n_a^2 |S(\mathbf{g})|^2 e^{-g^2 u_T^2}}{m^2(1+g^2R^2)^2 g^3},$$

where two-dimensional angles $\mathbf{\Psi}$ and $\mathbf{\Theta}$ describe the angular spread in the beam of emitting electrons and the angular distribution of emitted photons respectively, $\Psi^2 = \Psi_\parallel^2 + \Psi_\perp^2$, $\Theta^2 = \Theta_\parallel^2 + \Theta_\perp^2$, the angle θ' describing the possible turning of the crystay by the goniometer is outlined in Fig.1, γ is the Lorentz-factor of emitting electron, the energy of emitted photon ω is assumed to be large as compared with the critical energy $\gamma\omega_0$ determining the manifestation of the density effect in PXR [14].

Let us consider the orientational dependence of strongly collimated PXR ($\Theta^2 \ll \gamma^{-2}$) from electron beam crossing a thin enough crystal (the multiple scattering angle Ψ_{tot} achievable at the exit of the target is assumed to be small as compared with γ^{-1}). The simple formula follows from (3) in conditions under consideration

$$\frac{\mathrm{d}E}{\mathrm{d}t\ \mathrm{d}^2\Theta} = E_0\gamma^2 g F_0(2\gamma\theta', \gamma\varphi), \tag{4}$$
$$F_0 = \frac{\gamma^2\varphi^2}{1+\gamma^2\varphi^2} \frac{\left(2\gamma\theta' - \frac{1}{\gamma\varphi}\right)^2}{(1+4\gamma^2\theta'^2)^2}$$

Obviously, in the limit $\gamma\varphi \to \infty$ the dependence $F_0(2\gamma\theta')$ is reduced to well known in PXR theory curve with two symmetrical maxima. On the other hand, amplitudes of these maxima differ essentially from each other in the range of small orientation angles, as may be seen from Fig.2. The discussed asymmetry implies that the most part of emitted PXR photons is concentrated in the narrow range of observation angles close to the left-hand maximum in PXR angular distribution. It is of first importance that the amplitude of this maximum increases with decreasing of the orientation angle $\varphi/2$. Thus, the possibility to increase substantially PXR angular density can be realized in the range of grazing incidence of emitting electrons on the reflecting crystallographic plane of the crystalline target.

In circumstances where $\varphi \ll 1$ special attention must be given to PXR spectral density. Integrating (3) over observation angles allows

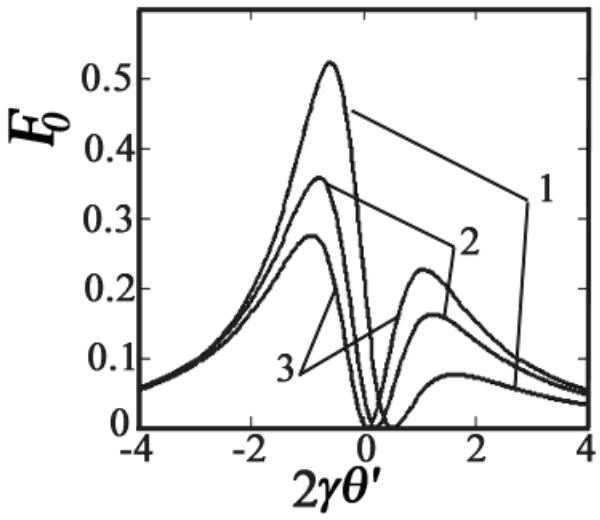

Figure 2. Asymmetry of PXR orientational dependence. The presented function $F_0(2\gamma\theta')$ is connected with PXR angular density by Eq.4. The curves 1,2,3 have been calculated for $\gamma\varphi = 2,\ 5,\ 20$ respectively.

one to obtain in the case of strongly collimated radiation $\Theta_d \ll \varphi$ (Θ_d is the photon collimator angular size) best suited for our purposes the following expression for the spectrum of emitted energy

$$\begin{aligned}\frac{\mathrm{d}E}{\mathrm{d}t\ \mathrm{d}\omega} \approx E_0\gamma^{-1}&\frac{(2\gamma\theta' - \frac{1}{\gamma\varphi})^2}{(1+4\gamma^2\theta'^2)^2}\gamma^3\varphi^3\frac{\omega_B}{\omega}\\ &\times\sqrt{\frac{\Theta_d^2}{\varphi^2} - \left(1 - \sqrt{\frac{\omega_B}{\omega}\left(1+\frac{2\theta'}{\varphi}\right) - \frac{1}{\gamma^2\varphi^2}}\right)^2}\\ &\times\sigma\left[\frac{\omega}{\omega_B} - \frac{1+2\theta'/\varphi}{\left(1+\frac{\Theta_d}{\varphi}\right)^2 + \frac{1}{\gamma^2\varphi^2}}\right]\sigma\left[\frac{1+2\theta'/\varphi}{\left(1-\frac{\Theta_d}{\varphi}\right)^2 + \frac{1}{\gamma^2\varphi^2}} - \frac{\omega}{\omega_B}\right]\end{aligned} \tag{5}$$

where $\omega_B = g/\varphi$ is the Bragg frequency in the vicinity of which PXR spectrum is concentrated, $\sigma(x) = 1$ if $x > 0$ and $\sigma(x) = 0$ if $x < 0$.

As one would expect, amplitude of the spectrum (5) as a function of the angle θ' peaks at the value of θ' corresponding to maximum in the orientational dependence (4). In line with (5), the relative width of PXR

spectral peak

$$\frac{\Delta\omega}{\omega} \approx 4\frac{\gamma^2\varphi^2}{1+\gamma^2\varphi^2}\frac{\Theta_d}{\varphi} \tag{6}$$

increases with decreasing of φ in the range $\varphi \gg \gamma^{-1}$, but this growth is returned if φ becomes comparable with γ^{-1}.

The width (6) is determined by the collimator size Θ_d. In the real conditions this width may be changed due to multiple scattering of emitting electrons. In order to estimate an influence of multiple scattering on PXR properties one should average the general expression (3) over scattering angles. It is interesting to note in this connection that the representation of PXR spectral-angular distribution in the form (3) is very convenient for further analysis because the scattering angle $\mathbf{\Psi}$ appears in the argument of δ-function in (3) only.

Using the general formula

$$\frac{\mathrm{d}E}{\mathrm{d}\omega\ \mathrm{d}^2\Theta} = \int\limits_0^L \mathrm{d}t \int \mathrm{d}^2\Psi f(t,\mathbf{\Psi})\frac{\mathrm{d}E}{\mathrm{d}t\ \mathrm{d}\omega\ \mathrm{d}^2\Theta} \tag{7}$$

and the distribution function

$$f(t,\mathbf{\Psi}) = \frac{1}{\pi(\Psi_0^2+\Psi_S^2 t)}\exp\left[-\frac{\Psi^2}{\Psi_0^2+\Psi_S^2 t}\right], \tag{8}$$

where Ψ_0 is the initial angular spread of emitting electron beam, $\Psi_S = \frac{1}{\gamma}\sqrt{L_{Sc}}$ is the multiple scattering angle per unit length, $L_{\mathrm{Sc}} \approx e^2 L_{\mathrm{Rad}}/4\pi$, L_{Rad} is the radiation length, one can obtain the following formula for the emission spectral-angular distribution:

$$\frac{\mathrm{d}E}{\mathrm{d}\omega\ \mathrm{d}^2\Theta} = E_0\frac{\gamma L_{\mathrm{Sc}}}{2}\Phi\left[\frac{\omega}{\omega_{\mathrm{B}}}, \Theta, \theta', \gamma\varphi, \frac{L}{L_{\mathrm{Sc}}}\right], \tag{9}$$

with

$$\begin{aligned}\Phi &= \gamma\varphi\frac{\omega_{\mathrm{B}}}{\omega}\frac{\frac{\omega_{\mathrm{B}}}{\omega}\left[\frac{\omega_{\mathrm{B}}}{\omega}-1+\frac{2}{\varphi}(\theta'+\Theta_\parallel)\right]-\frac{1}{\gamma^2\varphi^2}}{\left[\frac{\omega_{\mathrm{B}}}{\omega}-1+\frac{2}{\varphi}(\theta'+\Theta_\parallel)\right]^2} \\ &\times\sigma\left[\frac{\omega_{\mathrm{B}}}{\omega}\left(\frac{\omega_{\mathrm{B}}}{\omega}-1+\frac{2}{\varphi}(\theta'+\Theta_\parallel)\right)-\frac{1}{\gamma^2\varphi^2}\right] \\ &\times\int\limits_{t_-}^{t_+}\frac{\mathrm{d}t}{\kappa(t)}\left[E_1\left(\frac{t^2+(\kappa-\Theta_\perp/\varphi)^2}{\Psi_0^2/\varphi^2+\gamma^2\varphi^2 L/L_{\mathrm{Sc}}}\right)\right.\end{aligned} \tag{10}$$

$$
\begin{aligned}
&-E_1\left(\frac{t^2+(\kappa-\Theta_\perp/\varphi)^2}{\Psi_0^2/\varphi^2}\right)\\
&+E_1\left(\frac{t^2+(\kappa+\Theta_\perp/\varphi)^2}{\Psi_0^2/\varphi^2+\gamma^2\varphi^2 L/L_{\rm Sc}}\right)-E_1\left(\frac{t^2+(\kappa+\Theta_\perp/\varphi)^2}{\Psi_0^2/\varphi^2}\right)\Bigg],\\
\kappa(t) &= \sqrt{(t_+-t)(t-t_-)},\\
t_\pm &= \frac{\omega_{\rm B}}{\omega}-1+\frac{\Theta_\parallel}{\varphi}\pm\sqrt{\frac{\omega_{\rm B}}{\omega}\left(\frac{\omega_{\rm B}}{\omega}-1+\frac{2}{\varphi}(\theta'+\Theta_\parallel)\right)-\frac{1}{\gamma^2\varphi^2}}
\end{aligned}
$$

Let us use the result (9) to study the influence of multiple scattering on the orientational dependence of strongly collimated emission. It should be noted that the formula (9) does not take into account an influence of photoabsorption of emitted photons, but small values of the angle φ correspond to large values of the Bragg frequency $\omega_B = g/\varphi$, so that the emission of weakly absorbed hard X–rays is considered actually in this section.

PXR spectrum (the function $\Phi(\omega/\omega_B)$) calculated by (9) in the maximum of orientational dependence ($\mathbf{\Theta} = 0, \quad 2\gamma\theta' = -\sqrt{1+1/\gamma^2\varphi^2} + 1/\gamma\varphi$) is illustrated by the curves presented in Fig.3 and Fig.4. The simplest case of an electron beam without initial angular spread ($\Psi_0 = 0$) is considered in this paper. The curves presented in Fig.3 illustrate the effect of substantial increase of PXR spectral width with decreasing the parameter $\gamma\varphi$. The effect of saturation of PXR spectral density due to an influence of multiple scattering with an increase in the thickness of the target is demonstrated by the curves presented in Fig.4.

An advantage of PXR emission mechanism discussed above consists in the possibility to generate X–rays in wide frequency range. On the other hand the intensity of PXR is not very high. More intensive source of X–rays can be created on the base of Cherenkov emission mechanism [8, 9] to be studied in the next section.

3. Cherenkov X–rays in conditions of grazing incidence of emitting electrons on the surface of a target

Cherenkov emission mechanism allows to generate soft X–rays in the vicinity of atomic absorption edges, where a medium refractive index may exceed unity [4]. This theoretical prediction has been experimentally confirmed [6–10]. Let us consider Cherenkov X–rays under special conditions of grazing incidence of emitting electrons on the surface of a target. We are interesting in the emission process in soft X–ray

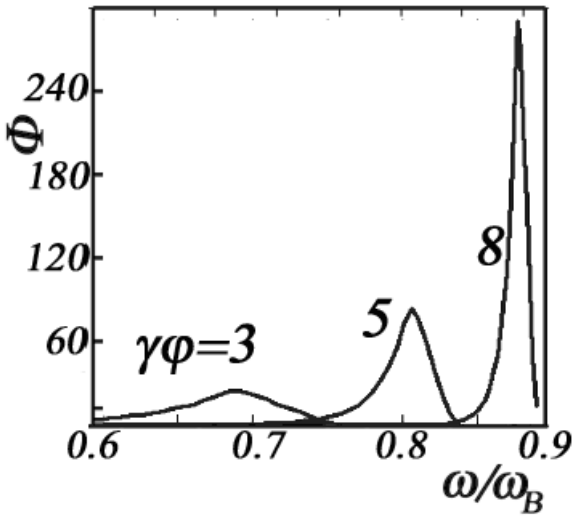

Figure 3. The growth of PXR spectral width with decreasing the incidence angle. The presented function Φ is connected with PXR spectral density by Eq.9. The curves have been calculated for fixed values of the parameters $\mathbf{\Theta} = 0$, $\Psi_0 = 0$, $2\gamma\theta' = -\sqrt{1 + 1/\gamma^2\varphi^2} + 1/\gamma\varphi$, $L/L_{Sc} = 0.3$ and different values of the parameter $\gamma\varphi$.

range of the emitted photon energies ω, where an influence of a photoabsorption is very important. Assuming that the photoabsorption length $l_{ab} \sim 1/\omega\chi''(\omega)$ (χ'' is the imaginary part of the dielectric susceptibility) is less than the electron path in the target L/φ (L is the thickness of the target, φ is the grazing incidence angle, $\varphi \ll 1$) we are led to the simple model corresponding to the emission of a fast electron moving from semi-infinite absorbing target to a vacuum where the emitted photons are recorded in X–ray detector (see Fig.5). Since background in the small frequency range under study is determined in the main by transition radiation, we neglect the contribution of bremsstrahlung. In addition to this we consider the emission from electrons moving with uniform velocity $\mathbf{v}$, assuming that the value of multiple scattering angle achievable on the distance of the order of l_{ab}, $\Psi_{ms} \sim \sqrt{L_{ab}/\gamma^2 L_{\rm Sc}}$ is small relative to characteristic angle of the Cherenkov cone $\sqrt{\chi'(\omega)}$ ($\chi'(\omega)$ is the real part of dielectric susceptibility).

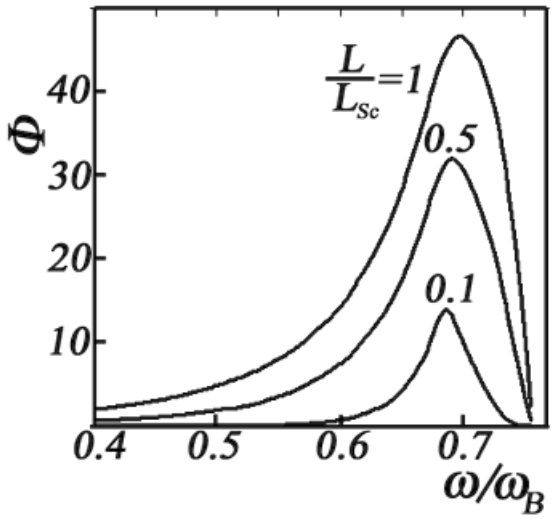

Figure 4. The saturation of PXR yield due to the influence of multiple scattering. The curves have been calculated for fixed values of the parameters $\gamma\varphi = 3$, $\mathbf{\Theta} = 0$, $\Psi_0 = 0$, $2\gamma\theta' = -\sqrt{1 + 1/\gamma^2\varphi^2} + 1/\gamma\varphi$ and different values of the parameter $L/L_{\rm Sc}$.

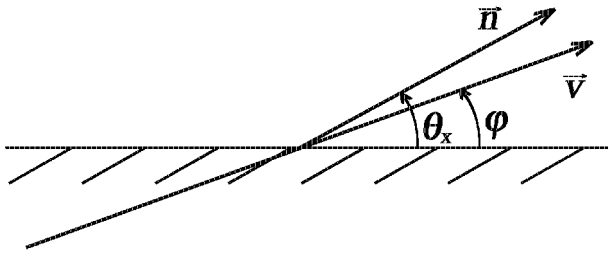

Figure 5. Geometry of the Cherenkov radiation process. **n** is the unit vector to the direction of emitted photon propagation, **v** is the emitting electron velocity, φ is the incidence angle.

Since the solution of the task under study is well known, we present the final result only

$$\frac{\mathrm{d}E}{\mathrm{d}\omega\ \mathrm{d}^2\Theta} = \frac{16e^2}{\pi^2}\frac{\chi'^2 + \chi''^2}{(\Theta_x + \tau')^2 + \tau''^2} \times \frac{\left[\gamma^{-2} + (\Psi_y - \Theta_y)^2 + \Theta_x^2 - \Psi_x^2\right]^2 + 4\Psi_x^2(\Psi_y - \Theta_y)^2}{\Omega_-^2\,\Omega_+^2} \tag{11}$$

$$\times \frac{\Psi_x^2 \Theta_x^2}{\left[\gamma^{-2} + (\Psi_y - \Theta_y)^2 + \Theta_x^2 + \Psi_x^2 - 2\Psi_x \tau'\right]^2 + 4\Psi_x^2 \tau"^2}$$

$$\tau' = \frac{1}{\sqrt{2}} \sqrt{\sqrt{(\Theta_x^2 + \chi')^2 + \chi"^2} + \Theta_x^2 + \chi'},$$

$$\tau'' = \frac{1}{\sqrt{2}} \sqrt{\sqrt{(\Theta_x^2 + \chi')^2 + \chi''^2} - \Theta_x^2 - \chi'},$$

where the angles $\mathbf{\Psi}$ and $\mathbf{\Theta}$ describe as above the angular spread of the beam of emitting electrons and the angular distribution of emitted photons respectively (see Fig.5), $\Omega_\pm = \gamma^{-2} + (\Psi_y - \Theta_y)^2 + (\Psi_x \pm \Theta_x)^2$.

The formula (11) allows to search the dependence of the total emission distribution on the value of incidence angle Ψ_x. Within the range of small Ψ_x under consideration multiple scattering of emitting electrons in the target can influence substantially on emission properties. To account such influence one should average the expression (11) over Ψ_x and Ψ_y. We use in this work the simple distribution function

$$f(\Psi_x, \Psi_y) = \frac{1}{\pi \Psi_L^2} \exp\left[-\frac{\Psi_y^2 + (\Psi_x - \varphi)^2}{\Psi_L^2}\right], \tag{12}$$

where $\Psi_L = \sqrt{L/\gamma^2 L_{Sc} \varphi}$ is the multiple scattering angle achievable at the electron path in the target L/φ.

As will be apparent from (11) the presented spectral-angular distribution contains a maximum (Cherenkov maximum), determined by the condition $\gamma^{-2} + (\Psi_y - \Theta_y)^2 + \Theta_x^2 + \Psi_x^2 - 2\Psi_x \tau' = 0$, which can be represented as

$$\gamma^{-2} - \chi' + \Theta_y^2 + \left(\varphi - \sqrt{\Theta_x^2 + \chi'}\right)^2 = 0 \tag{13}$$

in the most interesting for us frequency range of anomalous dispersion before absorption edge where χ'' is usually much less than χ' (as this takes place $\tau' \approx \sqrt{\Theta_x^2 + \chi'}$, $\tau'' \approx \frac{1}{2}\chi'' \Big/ \sqrt{\Theta_x^2 + \chi'}$) and the Cherenkov radiation can be realized if $\chi' - \gamma^{-2} > 0$ in accordance with (13) (this is well known Cherenkov threshold in X–ray range). An influence of multiple scattering is neglected in (13) as well.

Let us consider the angular structure of the Cherenkov peak versus the orientation angle φ. From (11) for large enough $\varphi \gg \sqrt{\chi'} > \gamma^{-1}$ the

emission angular distribution comprises two symmetric cones

$$\frac{\mathrm{d}E_0}{\mathrm{d}\omega\ \mathrm{d}^2\Theta} = \frac{e^2}{\pi^2}\frac{{\chi'}^2}{\left[\gamma^{-2} - \chi' + \Theta_y^2 + (\varphi - \Theta_x)^2\right]^2 + \chi''^2} \times \frac{\Theta_y^2 + (\varphi - \Theta_x)^2}{\left[\gamma^{-2} + \Theta_y^2 + (\varphi - \Theta_x)^2\right]^2} \tag{14}$$

The first of these radiation cones corresponding to the condition (13) represents Cherenkov radiation. Second one describes well known transition radiation. The structure of these cones is changed essentially when decreasing of the incidence angle φ. The distribution of emission intensity over azimuth angle on the Cherenkov cone becomes strongly non-uniform in contrast with (14). To show this let us compare the magnitudes of the distribution (11) in the plane $\Theta_y = 0$ at the points

$$\Theta_{x\,\max}^{(\pm)} = \sqrt{\left(\varphi \pm \sqrt{\chi' - \gamma^{-2}}\right)^2 - \chi'}, \tag{15}$$

following from (13) and corresponding to the maximum of the Cherenkov radiation intensity. Such magnitudes follow from (11) and (15)

$$\left.\frac{\mathrm{d}E_{\max}^{(\pm)}}{\mathrm{d}\omega\ \mathrm{d}^2\Theta}\right|_{\Theta_y=0} = \frac{4e^2}{\pi^2}\frac{\chi' - \gamma^{-2}}{\chi''^2}\frac{1}{\varphi^2} \times \left(\frac{1}{\varphi \pm \sqrt{\chi' - \gamma^{-2}}} + \frac{1}{\sqrt{\left(\varphi \pm \sqrt{\chi' - \gamma^{-2}}\right)^2 - \chi'}}\right)^{-2} \tag{16}$$

First of all it is necessary to note that two maxima (16) can be realized in the range of large enough values of $\varphi > \sqrt{\chi'} + \sqrt{\chi' - \gamma^{-2}}$ only, as it follows from (15). Obviously, the value of these maxima one the same for large enough $\varphi \gg \sqrt{\chi'}$ and coincide with that following from (14) $\left.\frac{\mathrm{d}E_{\max}^{(\pm)}}{\mathrm{d}\omega\ \mathrm{d}^2\Theta}\right|_{\Theta_y=0} = \frac{\mathrm{d}E_{0\,\max}}{\mathrm{d}\omega\ \mathrm{d}^2\Theta} = \frac{e^2}{\pi^2}\frac{\chi' - \gamma^{-2}}{\chi''^2}$.

In accordance with (15) only the maximum $\frac{\mathrm{d}E_{\max}^{(+)}}{\mathrm{d}\omega\ \mathrm{d}^2\Theta}$ is realized in the range $\sqrt{\chi'} - \sqrt{\chi' - \gamma^{-2}} < \varphi < \sqrt{\chi'} + \sqrt{\chi' - \gamma^{-2}}$ (the Cherenkov cone begins to contact with the target's surface if $\varphi = \sqrt{\chi'} + \sqrt{\chi' - \gamma^{-2}}$). The magnitude of this maximum can exceed substantially the asymptotic value $\frac{e^2(\chi' - \gamma^{-2})}{\pi^2(\chi''^2)}$. The ratio $\left(\frac{\mathrm{d}E_{\max}^{(+)}}{\mathrm{d}\omega\ \mathrm{d}^2\Theta} \Big/ \frac{\mathrm{d}E_{0\,\max}}{\mathrm{d}\omega\ \mathrm{d}^2\Theta}\right)$, as the performed analysis

of the expression (16) implies, depends strongly on the parameter $\gamma^2\chi'$. For example, this ratio has a value of about 10 if $\gamma^2\chi' = 5$.

The result obtained is of great importance for the creation of an effective Cherenkov based X–ray source. Indeed, Cherenkov emission mechanisms allow to generate very intensive soft X–ray beams (a yield of the order of 10^{-3} photons/electron has been obtained experimentally from a single foil [8, 9]). On the other hand, the angular density of Cherenkov radiation is not high since Cherenkov photons are emitted in a hollow cylindrical cone with a relatively large characteristic angle $\Theta_{Ch} \sim \sqrt{\chi'}$ to the electron trajectory. To obtain a uniform angular distribution of the emitted photons one must extract a small part of Cherenkov cone by the photon collimator. As a consequence, the useful part of the total emission yield is reduced substantially. In the range of small incidence angles $\varphi \ll 1$, the distribution of Cherenkov photons over azimuth angle becomes strongly non-uniform. Therefore the possibility to increase the used part of emission yield is opened by placing of photon collimator at the point corresponding to the maximum of the angular density of Cherenkov radiation. Such possibility is demonstrated by Fig.6, where the angular distribution of Cherenkov radiation calculated by the formula (11) for fixed photon energy is presented.

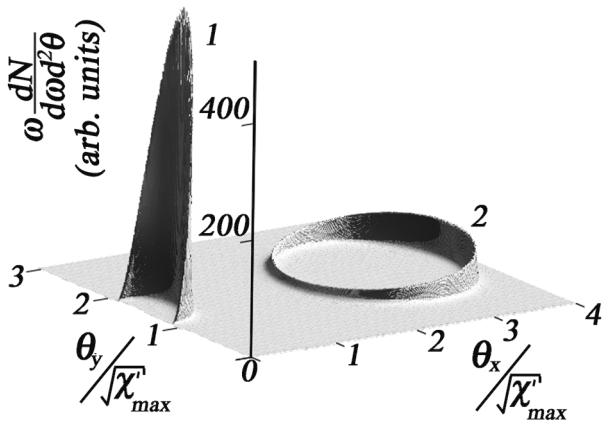

Figure 6. The dependence of Cherenkov cone structure on the incidence angle φ. The presented spectral-angular distributions of Cherenkov radiation have been calculated for Be target, $\omega = 111.6\ eV$ $1/\gamma\sqrt{\chi'_{\max}} = 0.4$, $\chi'_{\max} = 0.05$. Distribution 1 corresponds to the value of $\varphi = 0.17\sqrt{\chi'_{\max}}$. Distribution 2 corresponds to $\varphi = 3\sqrt{\chi'_{\max}}$.

As illustrated in Fig.6, there is not only the effect of non-uniform distribution of emitted photons over azimuth angle, but the effect of decreasing of Cherenkov emission angle when decreasing of the incidence angle φ as well. The effect in question have the simple geometrical interpretation [15]. As is clear from Fig.5 a photon emitted at the angle $\Theta^{(+)}_{x\,\max} > \varphi$ has a shorter path $L_{\rm ph}$ in the target than that of $L_{\rm el}$ emitting electron. This effect is small for large orientational angles $\varphi \gg \sqrt{\chi'}$. The photon yield is formed in this case at the part of electron inside trajectory of the order of absorption length $l_{ab} \sim 1/\omega\chi''$. On the other hand in the range of small $\varphi < \sqrt{\chi'}$ the ratio $L_{\rm el}/L_{\rm ph} \sim L_{\rm el}/L_{ab} \sim \Theta^{(+)}_{x\,\max}/\varphi$ is increased substantially in accordance with (16), which is to say that the useful part of electron trajectory and consequently the photon yield are increased. Geometrical interpretation allows us to explain both azimuth non-uniformity of the angular distribution of emitted photons (photon path in the target is increased with increasing azimuth angle) and the effect of "Cherenkov angle" decreasing.

It should be noted that the degree of non-uniformity in the emission angular distribution over azimuth angle depends strongly on the value of incidence angle φ. The great importance of correct choice of φ is demonstrated by the curves presented in Fig.7. These curves describing the ratio $\left(\frac{{\rm d}E^{(+)}_{\max}}{{\rm d}\omega\ {\rm d}^2\Theta} \Big/ \frac{{\rm d}E_{0\,\max}}{{\rm d}\omega\ {\rm d}^2\Theta}\right)$ as a function of φ have been calculated by the formula (16) for different values of the parameter $\gamma^2\chi'$.

Cherenkov X–ray radiation yield from Be target has been calculated in this work by the use general formula (11) and dielectric susceptibilities $\chi'(\omega)$ and $\chi''(\omega)$ determined experimentally [16]. The curves presented Fig.8 describe the spectra of Cherenkov photons, emitted from the above mentioned target into the collimator with finite angular size. The collimator's center was placed in performed calculations at the point corresponding to maximum of the emission angular density. Its angular size was chosen so that the emission yield in such a collimator was close to saturation for small incidence angle φ when the emission angular distribution over azimuth angle was strongly non-uniform. The presented curves demonstrate the substantial growth of the emission yield when decreasing of the incidence angle φ.

It should be noted that the emission angular density increases very substantially when increasing emitting particle energy, but this growth is followed by decreasing of optimum value of incidence angle φ (see Fig.7). Along that the influence of multiple scattering of emitting electrons in the target increases as well. Obviously such influence must constrain the discussed growth of the emission angular density. We have calculated the spectral-angular distribution of Cherenkov radiation from Be target on

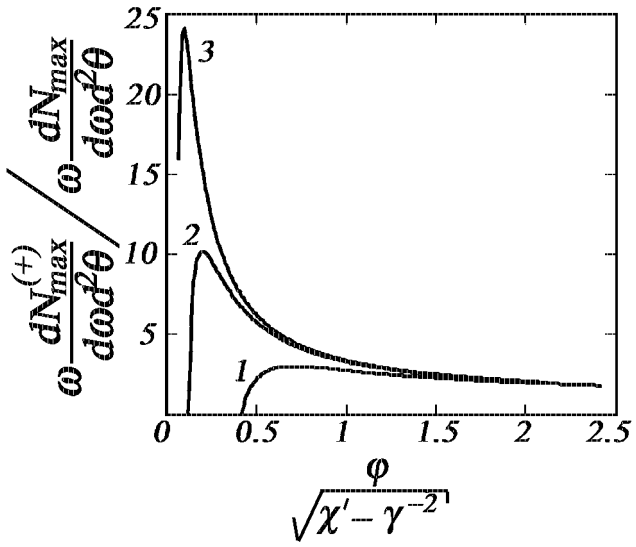

Figure 7. The amplification factor for Cherenkov angular density as a function of the incidence angle φ. The curves 1, 2 and 3 correspond to the value of the parameter $\gamma^2\chi' = 2,\ 5$ and 10 respectively.

the basis of the formula (11) averaged over beam spread at the exit of the target using the distribution function (12). The result of calculations, presented in Fig.9, shows a strong suppression of the angular density of Cherenkov radiation due to multiple scattering (this is because of very small angular width of Cherenkov cone proportional to χ'' as follows from (16)). On the other hand, the yield fixed by a photon collimator with finite angular size is not changed substantially as it is evident from the Fig.10.

Comparison of above considered X–ray sources based on PXR and Cherenkov mission mechanisms shows that PXR has an advantage over Cherenkov source consisting in the emission angle. This property allows to arrange an irradiated sample in the immediate vicinity of the source. The possibility to integrate properties of PXR and Cherenkov radiation sources into a single pattern is studied in the next section of the paper devoted to X–ray emission from relativistic electrons crossing a multilayer nanostructure under conditions when Cherenkov radiation can be realized.

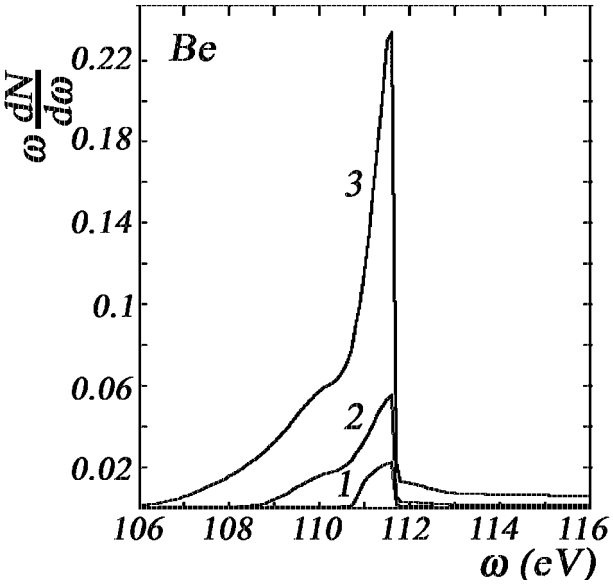

Figure 8. The spectrum of Cherenkov radiation from Be target as a function of the of the incidence angle φ. The curves have been calculated for Be target, $1/\gamma\sqrt{\chi'_{\rm max}} = 0.1$, $\chi'_{\rm max} = 0.05$, the collimator angular sizes $\Delta\Theta_x = 0.3\sqrt{\chi'_{\rm max}}$, $\Delta\Theta_y = 0.3\sqrt{\chi'_{\rm max}}$. Curves 1, 2 and 3 corresponds to $\varphi = 5\sqrt{\chi'_{\rm max}}$, $0.5\sqrt{\chi'_{\rm max}}$ and $0.05\sqrt{\chi'_{\rm max}}$ respectively.

4. Cherenkov X–rays from relativistic electrons crossing a multilayer nanostructure

Consider X–ray emission from relativistic electrons moving in a medium with a periodic dielectric susceptibility $\chi(\omega, \mathbf{r}) = \chi_0(\omega) + \sum_{\mathbf{g}}{}' \chi_{\mathbf{g}}(\omega)\, \mathrm{e}^{\mathrm{i}(\mathbf{g},\mathbf{r})}$. In the case of a one-dimensional structure consisting of alternative layers with thicknesses a and b and susceptibilities $\chi_a(\omega)$ and $\chi_b(\omega)$, respectively, the quantities $\chi_0(\omega)$ and $\chi_{\mathbf{g}}(\omega)$ are determined by the expressions

$$\chi_0(\omega) = \frac{a}{T}\chi_a + \frac{b}{T}\chi_b,$$

$$\chi_{\mathbf{g}}(\omega) = \frac{1 - \mathrm{e}^{\mathrm{i}(\mathbf{g},\mathbf{a})}}{\mathrm{i}gT}(\chi_a - \chi_b), \qquad (17)$$

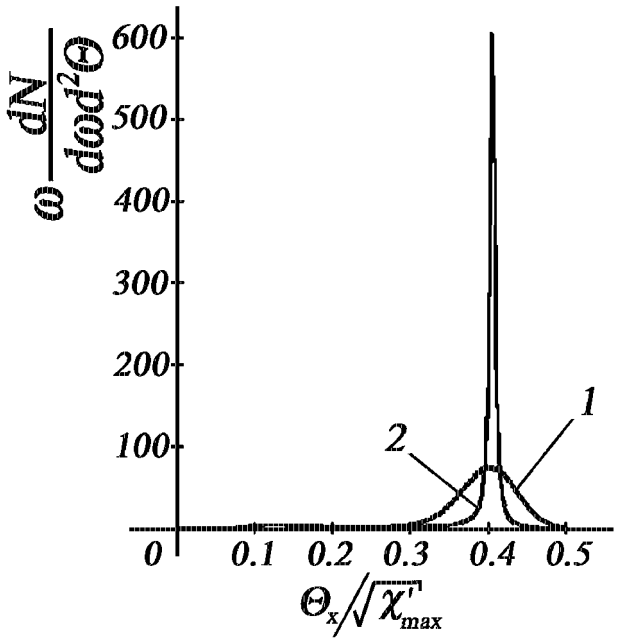

Figure 9. An influence of the multiple scattering on the Cherenkov radiation spectral-angular distribution. The curves 1 and 2 have been calculated with and without account of the multiple scattering respectively. The curves calculated for $1/\gamma\sqrt{\chi'_{\max}} = 0.04$, $\varphi = 0.08\sqrt{\chi'_{\max}}$.

where $T = a + b$ is the period of multilayer structure, $\mathbf{g} = \mathbf{e}_x g, \quad g \equiv g_n = \frac{2\pi}{T} n, \quad n = 0, \pm 1, \ldots$, $\mathbf{e}_x$ is the normal to the surface of a target (see Fig.11).

This task was under study in connection with the problem of X–ray source creation based on PXR and diffracted transition radiation from relativistic electrons crossing a multilayer nanostructure. The general solution obtained within the frame of dynamical diffraction theory can be found in [17], where an emission process in the range of hard X–rays far from photoabsorption edges has been considered. In contrast to this, soft X–ray generation in the vicinity of a photoabsorption edge is analyzed in this work. PXR properties can be changed substantially in this case due to the occurrence of Cherenkov radiation [18].

Embarking on a study of emission properties one should note that only Bragg scattering geometry can be realized in the case under consideration. Since soft X–rays are strongly absorbed in a dense medium,

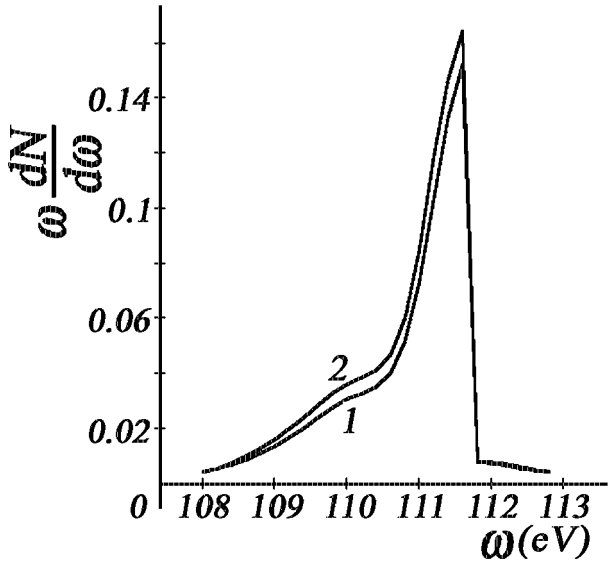

Figure 10. An influence of the multiple scattering on the Cherenkov radiation spectral distribution. The curves 1 and 2 have been calculated with and without account of the multiple scattering respectively. The curves have been calculated for *Be* target, $1/\gamma\sqrt{\chi'_{\max}} = 0.11$, $\chi'_{\max} = 0.05$, the collimator angular sizes $\Delta\Theta_x = 0.2\sqrt{\chi'_{\max}}$, $\Delta\Theta_y = 0.3\sqrt{\chi'_{\max}}$ and incidence angle $\varphi = 0.1\sqrt{\chi'_{\max}}$.

the simple model of semi-infinite multilayer nanostructure can be used for calculations. Keeping in mind fundamental aspects of the discussed problem only, we shall restrict our consideration to the specific case of the emitting electron moving with a constant velocity $\mathbf{v} = \mathbf{e}_1(1 - \frac{1}{2}\gamma^{-2})$ (see formulae (2)). Determining the unit vector $\mathbf{n}$ to the direction of emitted photon propagation by the formula (2) and using general results [17, 19] one can obtain the following expression for the spectral-angular distribution of emitted energy

$$\frac{\mathrm{d}E}{\mathrm{d}\omega\ \mathrm{d}^2\Theta} = \sum_{\lambda=1}^{2} |A_\lambda|^2, \tag{18}$$

where

$$A_\lambda \quad = \quad \frac{e}{\pi}\Theta_\lambda \frac{(\chi'_g + \mathrm{i}\chi''_g)\alpha_\lambda}{\Delta - \chi'_0 + \delta'_\lambda - \mathrm{i}(\chi''_0 + \delta''_\lambda)}$$

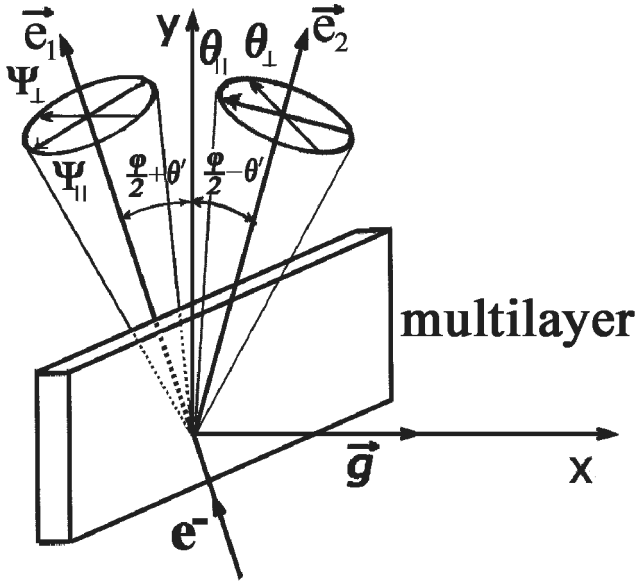

Figure 11. Cherenkov X–ray radiation from a multilayer X–mirror. Designations are the same as in Fig.1

$$\times \left[\frac{1}{\gamma^{-2} + \Theta^2 - \Delta - \delta'_\lambda + i\delta''_\lambda} - \frac{1}{\gamma^{-2} + \Theta^2} \right], \tag{19}$$

$$\Delta = 2\sin^2\left(\frac{\varphi}{2}\right)\left[1 - \frac{\omega}{\omega_B} + (\theta' + \Theta_\parallel)\cot\frac{\varphi}{2}\right],$$

$$\alpha_1 = 1, \qquad \alpha_2 = \cos\varphi,$$

and

$$\begin{aligned}
\delta'_\lambda &= \frac{\mathrm{sign}(D_\lambda)}{\sqrt{2}}\sqrt{\sqrt{C_\lambda^2 + D_\lambda^2} + C_\lambda}, \\
\delta''_\lambda &= \frac{1}{\sqrt{2}}\sqrt{\sqrt{C_\lambda^2 + D_\lambda^2} - C_\lambda}, \\
C_\lambda &= (\Delta - \chi'_0)^2 - (\chi'^{\,2}_g - \chi''^2_g)\alpha_\lambda^2 - \chi''^2_0, \\
D_\lambda &= 2[\chi''_0(\Delta - \chi'_0) + \chi'_g\chi''_g\alpha_\lambda^2],
\end{aligned}$$

with $\Theta_1 = \Theta_\perp$, $\Theta_2 = 2\theta' + \Theta_\parallel$, $\Theta^2 = \Theta_1^2 + \Theta_2^2$, and χ'_0, χ''_0 the real and imaginary part of the average dielectric susceptibility χ_0. The Bragg frequency is $\omega_\mathrm{B} = g/2\sin(\varphi/2)$, and finally $\chi'_g = \left(\sin\left(\pi\frac{a}{t}\right)/\pi\right)(\chi'_a - \chi'_b)$, and $\chi''_g = \left(\sin\left(\pi\frac{a}{t}\right)/\pi\right)(\chi''_a - \chi''_b)$.

The total emission amplitude A_λ in (18) can be represented in the form

$$\begin{aligned} A_\lambda &= A_\lambda^{\rm PXR} + A_\lambda^{\rm DTR}, \\ A_\lambda^{\rm PXR} &= \frac{e}{\pi}\frac{\Theta_\lambda}{\gamma^{-2}+\Theta^2-\chi_0'-{\rm i}\chi_0''}\frac{(\chi_g'+{\rm i}\chi_g'')\alpha_\lambda}{\gamma^{-2}+\Theta^2-\Delta-\delta_\lambda'+{\rm i}\delta_\lambda''}, \\ A_\lambda^{\rm DTR} &= -\frac{e}{\pi}\Theta_\lambda\left[\frac{1}{\gamma^{-2}+\Theta^2}-\frac{1}{\gamma^{-2}+\Theta^2-\chi_0'-{\rm i}\chi_0''}\right] \\ &\quad\times\frac{(\chi_g'+{\rm i}\chi_g'')\alpha_\lambda}{\Delta-\chi_0'+\delta_\lambda'-{\rm i}(\chi_0''+\delta_\lambda'')}, \end{aligned} \tag{20}$$

where $A_\lambda^{\rm PXR}$ describes the contribution of parametric X–rays, whereas A_λ^{DTR} is the amplitude of diffracted transition radiation [19]. It is clear that the Cherenkov like contribution to total emission yield is determined by the terms in (20) characterized by pole like singularity. Obviously, DTR amplitude has no poles (Cherenkov pole $\gamma^{-2}-\chi_0+\Theta^2=0$ is spurious because it disappears due to an interference between DTR and PXR, the reflection coefficient described by the last factor in the formula for $A_\lambda^{\rm DTR}$ has no poles close to real axis, as is easy to see taking into account the structure of the coefficients δ_λ and C_λ from (18)). Thus, the possible contribution of diffracted Cherenkov radiation is determined by PXR emission amplitude only, because the equality $\gamma^{-2}+\Theta^2-\Delta-\delta_\lambda=0$ can be fulfilled.

Let us consider the field of existence of the maximum in PXR reflex neglecting initially the influence of photoabsorption ($\chi_0''=\chi_g''=0$). The equation of PXR maximum realization

$$\begin{aligned} &\Delta_0-\Delta'-{\rm sign}(\Delta')\sqrt{\Delta'^2-\chi_g^2\alpha_\lambda^2}=0 \\ &\Delta_0=\gamma^{-2}-\chi_0+\Theta^2, \qquad \Delta'=\Delta-\chi_0 \end{aligned} \tag{21}$$

has the solution

$$\Delta'=\frac{\Delta_0^2+\chi_g^2\alpha_\lambda^2}{2\Delta_0} \tag{22}$$

in two non-overlapping ranges of the values of the parameter Δ_0.

The first of them determined by the inequality

$$\Delta_0>|\chi_g\alpha_\lambda| \tag{23}$$

corresponds to the branch of ordinary PXR. The second one determined by the inequality

$$\Delta_0<-|\chi_g\alpha_\lambda| \tag{24}$$

corresponds to Cherenkov branch of PXR. This radiation can appear only with the proviso that the Cherenkov condition $\Delta_0 < 0$ is fulfilled.

Since $|\Delta'| > |\chi_g \alpha_\lambda|$ as it is obvious from (22), both branches are realized outside the region of anomalous dispersion. Radiation corresponding to these branches can appear inside the region of anomalous dispersion $|\Delta'| < |\chi_g \alpha_\lambda|$ having regard to photoabsorption, but the yield of this radiation is small, as the performed analysis has shown.

Let us estimate the greatest possible spectral angular density of the discussed emission mechanism. By assuming that $\chi''_{0,g} \ll \chi'_{0,g}$, one can obtain from (18) the following simple formula

$$\begin{aligned} \left(\frac{\mathrm{d}N_\lambda}{\mathrm{d}\omega\ \mathrm{d}^2\Theta}\right)_{\max} &\approx \frac{e^2}{\pi^2}\frac{1}{\omega}\left(\frac{\chi'_g\alpha_\lambda}{\Delta_0}\right)^2\left(\frac{\Theta_\lambda}{\delta''_\lambda}\right)^2, \qquad (25)\\ \delta''_\lambda &= \chi''_0\left|\frac{\Delta_0^2+(\chi'_g\alpha_\lambda)^2}{\Delta_0^2-(\chi'_g\alpha_\lambda)^2}\right| - \chi''_g\alpha_\lambda\left|\frac{2\Delta_0\chi'_g\alpha_\lambda}{\Delta_0^2-(\chi'_g\alpha_\lambda)^2}\right|,\\ \Delta_0 &< -\chi'_g\alpha_\lambda\sqrt{1-\left(2\frac{\chi''_0-\chi''_g\alpha_\lambda}{\chi'_g\alpha_\lambda}\right)^{\frac{2}{3}}} \approx -\chi'_g\alpha_\lambda, \end{aligned}$$

describing the Cherenkov branch of PXR.

Obviously, the density (25) and that for ordinary Cherenkov radiation are of the same magnitude in the frequency range, where $|\Delta_0| \geq |\chi'_g\alpha_\lambda|$. Thus, the discussed emission mechanism based on self-diffracted Cherenkov radiation is of interest for X–ray source creation.

The structure of emitted photon flux calculated by the general formula (18) for $Be - C$ multilayer nanostructure is illustrated by the curves presented in Fig.12 and Fig.13. The period of nanostructure T and the orientation angle $\varphi/2$ were chosen so that the Bragg frequency ω_B and the frequency corresponding to maximum in real part of Be dielectric susceptibility were close to each other. Presented figures demonstrate the strong dependence of the emission angular distribution on the orientation angle. Distribution presented in Fig.12 has been calculated for fixed energies of emitting electrons and emitted photons. Large value of the angle $\varphi > \pi/2$ has been used in the performed calculations. On the other hand, distribution presented in Fig.13 has been calculated for the small values of the angle $\varphi < \pi/2$. It is crucial for the purposes of X–ray source creation that the presented distributions are strongly non-uniform. This property analogous to that discussed in the previous sections of the paper allows to increase the yield of strongly collimated radiation.

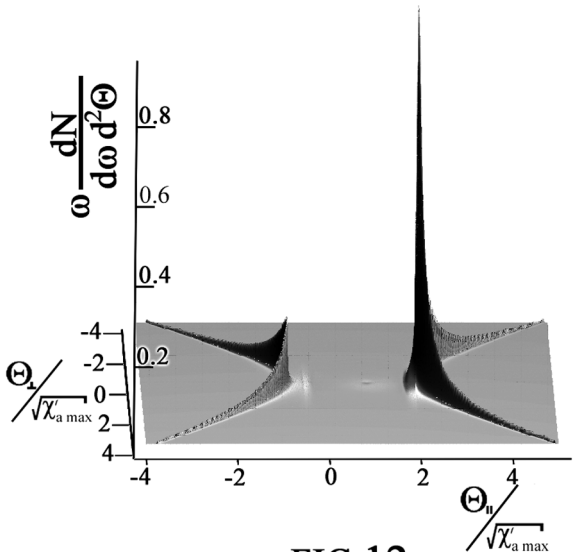

Figure 12. Spectral-angular distribution of Cherenkov radiation from multilayer X–mirror. The curve has been calculated for the fixed values of the parameters: $1/\gamma\sqrt{\chi'_{a\,\max}} = 0.2$, $\theta'/\sqrt{\chi'_{a\,\max}} = 0.53$, $\omega_B = \omega = 111.6$eV, $\varphi = 162^\circ$, $a/T = 0.9$, $\chi'_{a\,\max} = 0.05$ (Be).

5. Relative contribution of free and virtual photons to the formation of PXR yield

It should be noted that the model of PXR process used in above calculations does not take into account the contribution of real photons of diffracted bremsstrahlung to the formation of total emission yield since PXR cross-section was calculated for rectilinear trajectory of emitting electrons. As a consequence, only the contribution of actually parametric X–rays appearing due to the Bragg diffracted of virtual photons of the fast electron Coulomb field was taken into consideration in the performed analysis.

The discussed question concerning the relative contributions of indicated emission mechanisms to total emission yield is of interest for the problem of PXR based X–ray source creation because recent experiments [10, 11] pointed to a discrepancy between obtained data and the theory based on averaging of the ordinary PXR cross-section over multiple scattering angles. An exact statement of the discussed problem based on the kinetic equation approach was used in work [20]. Unfortunately, the expansions used in [20] allow to describe the case of thin enough target only, when the influence of multiple scattering is small. Currently the

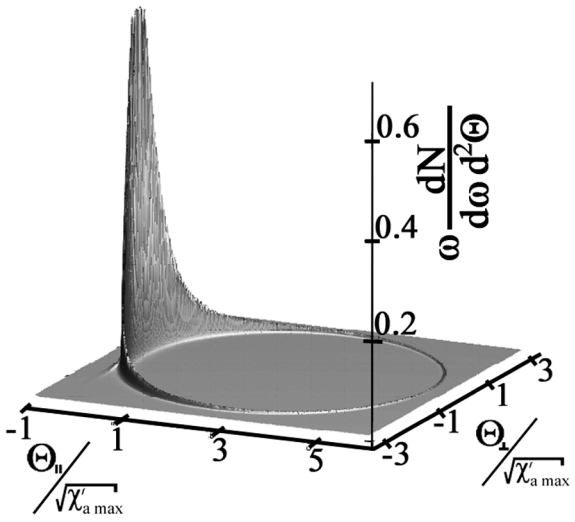

Figure 13. The same but for $\theta'/\sqrt{\chi'_{a\ \max}} = 0.7,\ \varphi = 44°$.

exact approach was used to analyze the influence of multiple scattering on the PXR spectral width [21, 22], but the question providing the subject matter for the present section.

Let us consider PXR process in more detail as compared with that in previous section of this paper. Starting from well known equations of dynamical diffraction theory [23]

$$(k^2 - \omega^2(1+\chi_0))\mathbf{E}_{\omega\mathbf{k}} - \mathbf{k}(\mathbf{k}, \mathbf{E}_{\omega\mathbf{k}}) - \omega^2 \sum_{\mathbf{g}}{}' \chi_{-\mathbf{g}}(\omega)\mathbf{E}_{\omega\mathbf{k}+\mathbf{g}} = 4\pi \mathrm{i}\omega \mathbf{J}_{\omega\mathbf{k}} \tag{26}$$

where $\mathbf{E}_{\omega\mathbf{k}}$ is the Fourier-transform of the electric field, χ_0 and χ_g are the components of the crystalline dielectric susceptibility $\epsilon(\omega, \mathbf{r}) = 1 + \chi_0(\omega) + \sum_{\mathbf{g}}{}' \chi_{\mathbf{g}} \mathrm{e}^{\mathrm{i}(\mathbf{g},\mathbf{r})}$, $\mathbf{J}_{\omega\mathbf{k}}$ is the Fourier-transform of the emitting electron current density, one can obtain on the basis of well known methods [23] the following expression for an emission field, propagating along the direction of Bragg scattering

$$\mathbf{E}_{\lambda\mathbf{k}+\mathbf{g}} = \frac{4\pi \mathrm{i}\omega^3 \chi_{\mathbf{g}} \alpha_\lambda}{D_\lambda} (\mathbf{e}_{\lambda\mathbf{k}}, \mathbf{J}_{\omega\mathbf{k}}), \tag{27}$$

$$D_\lambda = (k^2 - \omega^2(1+\chi_0))((\mathbf{k}+\mathbf{g})^2 - \omega^2(1+\chi_0)) - \omega^4 \chi_{\mathbf{g}} \chi_{-\mathbf{g}} \alpha_\lambda^2,$$

where $\mathbf{E}_{\omega\mathbf{k}+\mathbf{g}} = \sum\limits_{\lambda=1}^{2} \mathbf{e}_{\lambda\mathbf{k}+\mathbf{g}} E_{\lambda\mathbf{k}+\mathbf{g}}$, $\mathbf{e}_{\lambda\mathbf{k}}$ and $\mathbf{e}_{\lambda\mathbf{k}+\mathbf{g}}$ are the polarization vectors, $(\mathbf{k}, \mathbf{e}_{\lambda\mathbf{k}}) = (\mathbf{k}+\mathbf{g}, \mathbf{e}_{\lambda\mathbf{k}+\mathbf{g}}) = 0$, $\mathbf{g}$ is the reciprocal lattice vector (see Fig.11).

To determine an emission spectral-angular distribution one should calculate Fourier-integral $E_\lambda^{Rad} = \int d^3k_g \; e^{i(\mathbf{k}_g,\mathbf{n})r} E_{\lambda\,\mathbf{k}+\mathbf{g}}$ in the wave-zone by the stationary phase method (here $\mathbf{k}_g = \mathbf{k}+\mathbf{g}$, $\mathbf{n}$ is the unit vector to the direction of emitted photon propagation). The result of integration has the form

$$
\begin{aligned}
E_\lambda^{\mathrm{Rad}} &= \frac{4\pi^3 \mathrm{i}\omega^3 \chi_{\mathbf{g}} \alpha_\lambda}{\sqrt{\Delta'^2 + \omega^2 \chi_{\mathbf{g}} \chi_{-\mathbf{g}} \alpha_\lambda^2 (1-(\mathbf{n},\mathbf{g})/\omega)}} \qquad (28)\\
&\times \left[(\mathbf{e}_{\lambda\mathbf{k}_+}, \mathbf{J}_{\omega\mathbf{k}_+}) \mathrm{e}^{\mathrm{i}\xi_+ r} - (\mathbf{e}_{\lambda\mathbf{k}_-}, \mathbf{J}_{\omega\mathbf{k}_-}) \mathrm{e}^{\mathrm{i}\xi_- r} \right] \frac{\mathrm{e}^{\mathrm{i}\omega r}}{r},\\
\xi_\pm &= \frac{1}{2(1-(\mathbf{n},\mathbf{g})/\omega)} \left[-\delta' \pm \sqrt{\delta'^2 + \omega^2 \chi_{\mathbf{g}} \chi_{-\mathbf{g}} \alpha_\lambda^2 (1-(\mathbf{n},\mathbf{g})/\omega)} \right]\\
&\quad + \frac{\omega}{2} \chi_0,\\
\delta' &= \frac{g^2}{2\omega} - (\mathbf{n},\mathbf{g}) \left(1 + \frac{1}{2}\chi_0 \right), \quad \mathbf{k}_\pm = (\omega + \xi_\pm)\mathbf{n} - \mathbf{g}
\end{aligned}
$$

For the further analysis it is very convenient to introduce the angular variables $\mathbf{\Theta}$ and $\mathbf{\Psi}_t$ by the formulae analogous to (2).

Using (2) and (28) one can obtain the following expression for the spectral-angular distribution of the number of emitted photons:

$$
\begin{aligned}
\frac{\mathrm{d}N_\lambda}{\mathrm{d}\omega\, \mathrm{d}^2\Theta} &= \frac{e^2\omega |\chi_g|^2 \alpha_\lambda^2}{8\pi^2} \frac{1}{\delta^2 + \chi_g \chi_{-g} \alpha_\lambda^2 \cos\varphi}\\
&\times \mathrm{Re} \left\langle \int \mathrm{d}t \int\limits_0^\infty \mathrm{d}\tau \; \Omega_{\lambda\, t} \Omega_{\lambda\, t+\tau} \mathrm{e}^{-\mathrm{i}\omega\tau} \right.\\
&\times \left. \left[\mathrm{e}^{\mathrm{i}(\mathbf{k}_+, (\mathbf{r}_{t+\tau} - \mathbf{r}_t))} + \mathrm{e}^{\mathrm{i}(\mathbf{k}_-, (\mathbf{r}_{t+\tau} - \mathbf{r}_t))} \right] \right\rangle,
\end{aligned}
\qquad (29)
$$

where $\delta = \delta'/\omega_{\mathrm{B}}$, $\Omega_{1t} = \Theta_\perp - \Psi_{\perp t}$, $\Omega_{2t} = \Theta_\parallel + \Psi_{\parallel t} + 2\theta'$, θ' is the orientation angle (see Fig.11), the value $\theta' = 0$ corresponds to exact Bragg resonance orientation of the crystal relative to emitting electron velocity, the brackets $\langle\rangle$ mean the averaging over all possible trajectories of electrons in the target $\mathbf{r}_t \equiv \mathbf{r}(t)$, the angle $\mathbf{\Psi}_t$ is the time-dependent quantity because of multiple scattering. In accordance with (29) two

branches of propagating in the crystal electromagnetic waves take the contribution to total emission yield within the frame of used dynamical diffraction approach.

Procedure of averaging of the expressions analogous to (29) is described in book [3], where an influence of multiple scattering on the ordinary bremsstrahlung from relativistic electrons, moving in amorphous medium, has been considered in detail. Using the corresponding results [3] one obtain from (29) the final expression for the total emission intensity

$$\frac{\mathrm{d}N_\lambda}{\mathrm{d}t\,\mathrm{d}\omega\,\mathrm{d}^2\Theta} = \frac{e^2\omega|\chi_g|^2}{4\pi^2}\frac{\Omega_{\lambda\,t}^2\alpha_\lambda^2}{\sigma_\lambda^2}\mathrm{Re}\int\limits_0^\infty \mathrm{d}\tau \frac{\cos\left(\frac{\omega}{2}\sigma_\lambda\tau\right)}{\cosh^2(\sqrt{2\mathrm{i}\omega q}\tau)} \times \exp\left(-\frac{\mathrm{i}\omega}{2}(\gamma^{-2}-\chi_0-\delta)\tau - \sqrt{\frac{\mathrm{i}\omega}{8q}}\Omega_t^2\tanh(\sqrt{2\mathrm{i}\omega q}\tau)\right), \tag{30}$$

where $\sigma_\lambda^2 = \delta^2 + \chi_{\mathbf{g}}\chi_{-\mathbf{g}}\alpha_\lambda^2\cos\varphi, \quad q = 1/4L_{\mathrm{Sc}}\gamma^2$.

Let us use the general result (30) to elucidate the conditions such that the diffracted bremsstrahlung contribution can be substantial. The emission angular density

$$\frac{\mathrm{d}N}{\mathrm{d}^2\Theta} = \int\limits_0^L \mathrm{d}t \int \mathrm{d}^2\Psi_t\; f(t,\boldsymbol{\Psi}_t)\int\limits_0^\infty \mathrm{d}\omega \sum_{\lambda=1}^{2}\frac{\mathrm{d}N_\lambda}{\mathrm{d}t\,\mathrm{d}\omega\,\mathrm{d}^2\Theta} \tag{31}$$

in the most suitable characteristic for our purposes because this characteristic is very sensitive to the action of multiple scattering.

First of all let us integrate the intensity distribution (30) over emitted photon energies keeping in mind that the emission considered in this section is concentrated in the narrow vicinity of $\omega = \omega_{\mathrm{B}}$, because the Bragg diffraction process extracts this segment of initially wide spectra of both real photons of bremsstrahlung and virtual photons of the emitting electron Coulomb field. Taking into account that $\omega \approx \omega_{\mathrm{B}}$ in (30) except "fast variable" $\delta(\omega)$ (so-called resonance defect) one can perform the integration by the transformation of variables $\mathrm{d}\omega = \left(\frac{\mathrm{d}\delta}{\mathrm{d}\omega}\right)^{-1}\mathrm{d}\delta$. The result of integration has the following form

$$\frac{\mathrm{d}N_\lambda}{\mathrm{d}t\,\mathrm{d}^2\Theta} = -\frac{e^2\omega_{\mathrm{B}}^4|\chi_g|^2}{2\pi g^2}\frac{\Omega_{\lambda\,t}^2\alpha_\lambda^2}{\Omega_t^2\beta_\lambda}\mathrm{Im}\left\{\left[\beta_\lambda + \mathrm{i}\left(\frac{1}{\gamma^2}-\chi_0\right)\right]\right. \times \left.\int\limits_0^\infty \mathrm{d}\tau \exp\left[-\frac{\omega_{\mathrm{B}}}{2}\left[\beta_\lambda + \mathrm{i}\left(\frac{1}{\gamma^2}-\chi_0\right)\right]\tau\right.\right. \tag{32}$$

$$-\sqrt{\frac{\mathrm{i}\omega_\mathrm{B}}{8q}}\Omega_t^2\tanh\left(\sqrt{2\mathrm{i}\omega_\mathrm{B}q}\tau\right)\Bigg]\Bigg\},$$

where $\beta_\lambda^2=\chi_\mathbf{g}\chi_{-\mathbf{g}}\alpha_\lambda^2\cos\varphi$ (we are considering the parametric X–rays for Laue geometry, so $\varphi<\pi/2$).

The emission intensity (32) takes into account both parametric X–rays and diffracted bremsstrahlung contribution. To estimate the relative contribution of diffracted bremsstrahlung let us compare the exact result for the total emission angular density $\frac{\mathrm{d}N}{\mathrm{d}^2\Theta}$, following from (31) and (32), with that, following from the general formula (31) and simplified formula (32) corresponding to the emission from a fast electron moving with a constant velocity. The last case corresponds to the limit $q\to 0$ in (32), when this formula can be reduced to the ordinary PXR angular distribution

$$\frac{\mathrm{d}N_\lambda}{\mathrm{d}t\;\mathrm{d}^2\Theta}\to\frac{\mathrm{d}N_{0\lambda}}{\mathrm{d}t\;\mathrm{d}^2\Theta}=\frac{e^2\omega_\mathrm{B}^3|\chi_g|^2}{\pi g^2}\frac{\Omega_{\lambda\,t}^2\alpha_\lambda^2}{(\gamma^{-2}+\gamma_m^{-2}+\Omega_t^2)^2+\beta_\lambda^2},\tag{33}$$

where $\gamma_\mathrm{m}=\omega_\mathrm{B}/\omega_0$ (ω_0 is the plasma frequency).

Calculating the quantity $\frac{\mathrm{d}N}{\mathrm{d}^2\Theta}$ we have restricted our selves to the case of small incidence angle $\varphi\ll 1$, when $\alpha_2=\cos\varphi\approx\alpha_1=1$. Such conditions are most appropriate for the diffracted bremsstrahlung contribution to be substantial. Using the distribution function (8) and performing the integration in (31) over scattering angles $\mathbf{\Psi}_t$ one can obtain the following expression for $\mathrm{d}N/\mathrm{d}^2\Theta$:

$$\begin{aligned}\frac{\mathrm{d}N}{\mathrm{d}^2\Theta} &= \frac{e^2\omega_\mathrm{B}^3L_\mathrm{Sc}}{\pi g^2}F,\qquad(34)\\ F &= -\eta\,\mathrm{Im}\left\{\left(1+\frac{\gamma^2}{\gamma_\mathrm{m}^2}(1-\mathrm{i}\eta)\right)\int\limits_0^\infty\mathrm{d}t\,\coth(t)\right.\\ &\quad\times\exp\left[-\sqrt{\mathrm{i}}\left(1+\frac{\gamma^2}{\gamma_\mathrm{m}^2}(1-\mathrm{i}\eta)\right)\frac{\gamma_\mathrm{L}}{\gamma}t\right]\\ &\quad\times\left[E_1\left(\frac{\sqrt{\mathrm{i}}\gamma^2\Theta_0^2\frac{\gamma_L}{\gamma}\tanh(t)}{1+\sqrt{\mathrm{i}}\left(\frac{L}{L_\mathrm{Sc}}+\gamma^2\Psi_0^2\right)\frac{\gamma_L}{\gamma}\tanh(t)}\right)\right.\\ &\quad\left.\left.-E_1\left(\frac{\sqrt{\mathrm{i}}\gamma^2\Theta_0^2\frac{\gamma_\mathrm{L}}{\gamma}\tanh(t)}{1+\sqrt{\mathrm{i}}\gamma^2\Psi_0^2\frac{\gamma_L}{\gamma}\tanh(t)}\right)\right],\end{aligned}$$

where $\gamma_\mathrm{L}=\sqrt{\omega_\mathrm{B}L_\mathrm{Sc}/2},\ \eta=|\chi_g/\chi_0|<1,\ \Theta_0^2=\Theta_\perp^2+(2\theta'+\Theta_\parallel)^2$.

The function $F(\gamma\Theta_0)$ describing the contribution of both actually PXR and diffracted bremsstrahlung must be compared with analogous function

$$\begin{aligned} F_0 &= -\eta\,\mathrm{Im}\left\{\left(1+\frac{\gamma^2}{\gamma_\mathrm{m}^2}(1-\mathrm{i}\eta)\right)\right. \\ &\times\int_0^\infty \frac{\mathrm{d}t}{\sqrt{\left(1+\frac{\gamma^2}{\gamma_\mathrm{m}^2}(1-\mathrm{i}\eta)+\gamma^2\Theta_0^2+t\right)^2-4\gamma^2\Theta_0^2 t}} \\ &\left.\times\left[E_1\left(\frac{t}{\frac{L}{L_\mathrm{Sc}}+\gamma^2\Psi_0^2}\right)-E_1\left(\frac{t}{\gamma^2\Psi_0^2}\right)\right]\right\}, \end{aligned} \tag{35}$$

taking into account the contribution of PXR only and following from (37) and (33). The difference between these functions depends strongly on the parameters γ/γ_m and γ/γ_L. The physical meaning of the parameter $\gamma/\gamma_\mathrm{m} = \gamma\omega_0/\omega_\mathrm{B}$ is very simple. This parameter describes an influence of the density effect on PXR and bremsstrahlung emission mechanisms. Screening of the Coulomb field of emitting relativistic electron due to the density effect occurring in the range $\gamma > \gamma_\mathrm{m}$ is responsible for PXR yield saturation as a function of the energy of emitting electron [14]. Changing of an emitted photon phase velocity due to the polarization of medium electrons is responsible for bremsstrahlung yield suppression (Ter-Mickaelian effect [3]) in the frequency range $\omega < \gamma\omega_0$ (in the case $\omega \approx \omega_\mathrm{B}$ under consideration this inequality is equivalent to $\gamma > \gamma_\mathrm{m}$).

The parameter γ/γ_L describes an influence of another classical electrodynamical effect in the physics of high energy particle bremsstrahlung known as Landau-Pomeranchuk-Migdal effect (see [3]). LPM effect arises with the proviso that the multiple scattering angle of emitting particle Ψ_Coh achievable at the distance of the order of so-called formation length $l_\mathrm{Coh} \approx 2\gamma^2/\omega$ ($l_\mathrm{Coh} \approx 2\gamma^2/\omega_\mathrm{B}$ in the case in question) exceeds the characteristic emission angle of emitting particle $\Psi_\mathrm{em} \approx \gamma^{-1}$. Obviously, $\Psi_\mathrm{Coh}^2 = \frac{1}{\gamma^2 L_\mathrm{Sc}}\frac{2\gamma^2}{\omega_\mathrm{B}} = \gamma_L^{-2}$, so that $\gamma/\gamma_\mathrm{L} = \Psi_\mathrm{Coh}/\Psi_\mathrm{em}$ and therefore the condition $\gamma > \gamma_\mathrm{L}$ means LPM effect manifestation.

Let us consider the distribution $F(\gamma\Theta_0)$ in the range of small emitting particle energies $\gamma \ll \gamma_\mathrm{L}$. Close inspersion of the integral (34) shows that the effective values of the variable in integration $t_\mathrm{eff} \ll 1$ in conditions under consideration independently of the parameter γ/γ_m. Because of this, $\tanh(t) \approx t$ and the formula (34) can be reduced to more simple one

$$F \rightarrow -\eta\,\mathrm{Im}\left\{\left(1+\frac{\gamma^2}{\gamma_\mathrm{m}^2}(1-\mathrm{i}\eta)\right)\int\limits_0^\infty \frac{\mathrm{d}t}{t}\exp\left[-\left(1+\frac{\gamma^2}{\gamma_\mathrm{m}^2}(1-\mathrm{i}\eta)\right)t\right]\right.$$
$$\left.\times\left[E_1\left(\frac{\gamma^2\Theta_0^2 t}{1+\left(\frac{L}{L_\mathrm{Sc}}+\gamma^2\Psi_0^2\right)t}\right)-E_1\left(\frac{\gamma^2\Theta_0^2 t}{1+\gamma^2\Psi_0^2 t}\right)\right]\right\} \qquad (36)$$

The performed numerical analysis has shown that the function $F_0(\gamma\Theta_0)$ in (35) and the modified function $F(\gamma\Theta_0)$ in (36) coincide. By this means PXR characteristics are well described with the constraint $\gamma \ll \gamma_\mathrm{L}$ within the framework of ordinary PXR theory based on the calculation of PXR cross-section using the rectilinear trajectory of emitting particles. To explain this conclusion it is necessary to note that in conditions $\gamma \ll \gamma_\mathrm{L}$ under consideration the trajectory of emitting particle is close to stright line at the distance of the order of l_Coh for which the emitted photon is formed (the used expansion $\tanh(t) \approx t$ implies that the bend of electron's trajectory is neglected). As this takes place, the structure of the emitted electron electromagnetic field consisting of both virtual photons of the electron Coulomb and free photons of the bremsstrahlung is close to that for the electron moving along the rectilinear trajectory with a constant velocity. As a consequence, the structure of the diffracted by crystalline atomic planes electromagnetic field differs little from the ordinary PXR field.

In the opposite case $\gamma > \gamma_\mathrm{L}$ the velocity of emitting electron turns through the angle $\Psi_\mathrm{Coh} > \gamma^{-1}$ at the distance l_Coh. Since the value γ^{-1} is the scale if angular distribution of virtual photons associated with the electron's Coulomb field, the structure of total electromagnetic field of emitting electron differs substantially from that for the electron moving along the rectilinear trajectory. Because of this the structure of diffracted field is changed substantially as well. Relative contribution of diffracted bremsstrahlung depends in the case in question on the parameter γ/γ_m. This contribution is small if $\gamma > \gamma_m$ and bremsstrahlung is suppressed by Ter-Mikaelian effect. On the other hand, the contribution of diffracted bremsstrahlung can be very essential if $\gamma < \gamma_\mathrm{m}$, but $\gamma > \gamma_\mathrm{L}$ (obviously, both these inequalities can be valid simultaneously with the proviso that $\gamma_L < \gamma_\mathrm{m}$ only).

The discussed results are demonstrated by the Fig.14 and Fig.15, where the functions $F(\gamma\Theta_0)$ and $F_0(\gamma\Theta_0)$ calculated by the formula (34) and (35) respectively are presented. The curves presented in Fig.15 predict the dominant contribution of the diffracted bremsstrahlung to total emission yield under special conditions.

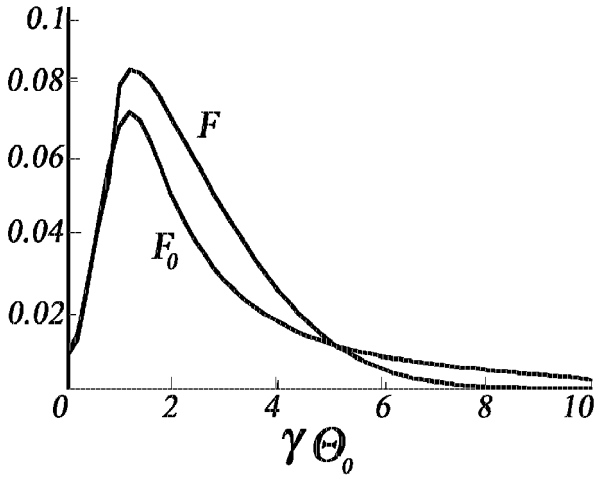

Figure 14. The emission angular density with and without diffracted bremsstrahlung contribution. The presented functions $F(x)$ and $F_0(x)$ defined by (32) and (33) have been calculated for fixed values of the parameters $L/L_{\rm sc} = 0.5$, $\eta = 0.8$, $\gamma_{\rm L}/\gamma_{\rm m} = 0.5$ and $\gamma_{\rm m}/\gamma = 5$.

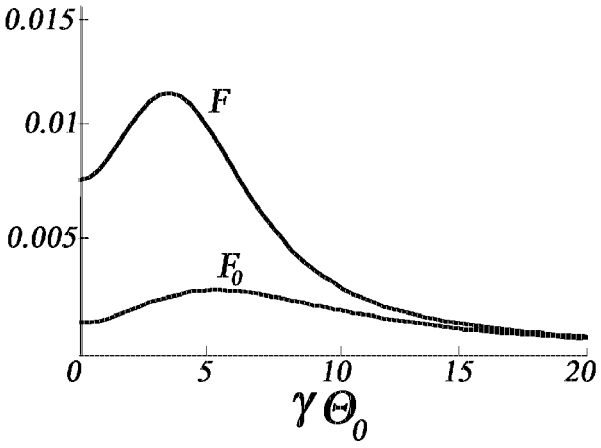

Figure 15. The same but for $\gamma_{\rm m}/\gamma = 0.3$.

6. Conclusions

Performed analysis has shown that the angular density of X–rays produced by X–ray sources based on Cherenkov and quasi-Cherenkov emission mechanisms can be increased substantially in conditions of grazing incidence of emitting electrons at the surface of a radiator, when the

angular distribution of emitted photons becomes strongly non-uniform. Owing to this fact, most part of emitted photons is concentrated in the small region of observation angles resulting in the high yield of collimated radiation.

In the case of Cherenkov X–ray source the discussed non-uniformity is caused by the strong dependence of a photoabsorption coefficient on the direction of emitted photon propagation. In accordance with performed calculations an increase in the emission angular density of the order of $5 - 10$ and more possible in the range of incidence angles of the order of Cherenkov emission angle.

The analogous enhancement of the emission angular density is possible for PXR source (in the case being considered the anisotropic angular distribution of emitted photons is caused by the dependence of PXR reflection coefficient on the photon energy and strong connection of this energy with the observation angle given by the condition of Bragg diffraction). On the other hand, the growth of PXR angular density with decreasing the emitting electron incidence angle relative to reflecting crystallographic plane of the crystalline target is attended by substantial growth of the spectral width of emitted photon flux.

Cherenkov X–ray radiation is possible not only in homogeneous media but in multilayer periodic nanostructure as well. An advantage of the last scheme consists in the possibility to generate X–rays at large angles relative to emitting electron velocity and consequently to arrange an irradiated sample in the immediate vicinity of the radiator. The performed calculations have shown the possibility to obtain in this scheme the intensity and angular density of emitting photons close to that achievable in the ordinary scheme used the homogeneous target.

Analysing the relative contributions from diffracted bremsstrahlung and PXR to the total emission yield from relativistic electrons crossing a crystal shows that diffracted bremsstrahlung can dominate under special conditions as elucidated in this note.

Acknowledgments

This work was supported by RFBR (grants:02-02-16941, 03-02-16263) and Program "DOPFIN" Russian Ministry of Science and Education. One of the authors (A.K.) is grateful to Russian Ministry of Education and CRDF (grant VZ-010-0) for financial support.

References

[1] Ginzburg V. and Frank I. *Emission from uniformly moving appared when crossing a boundary between two different media. J. Phys. USSR*, **9** p.353, 1945.

[2] Kumakhov M. *On the theory of electromagnetic radiation of charged particles in a crystal. Phys. Lett.*, **57**, p.17, 1976

[3] Ter-Mikaelian M. *High Energy Electromagnetic Processes in Condenced Media*, Wiley, New York, 1972.

[4] Bazylev V., Glebov V., Denisov E. et al. *JEPT Letters*, **24**, p.406, 1976.

[5] Rullhusen P., Artru X. and Dhez P. *Novel Radiation Sources Using Relativistic Electrons*, Word Scientific, Singapore, 1999.

[6] Bazylev V., Glebov V., Denisov E. et al. *JEPT*, **81**, p.1664, 1981.

[7] Moran M, Chang B., Schueider M. and Maruyama X. *Grazing-incidence Cherenkov X–ray generation. Nucl. Instr. Meth.*, B**48**, p.287, 1990.

[8] Knulst W., Luiten O., van der Wiel M. and Verhoeven J. *Observation of narrow band Si L-edge Cherenkov radiation generated by* 5 *MeV electrons. Appl. Phys. Lett.*, **79**, p.2999, 2001.

[9] Knulst W., van der Wiel M., Luiten O. and Verhoeven J. *High-brightness, narrow band and compact soft X–ray Cherenkov sources in the water window. Appl. Phys. Lett.*, **83**, p.1050, 2003.

[10] Knulst W., van der Wiel M., Luiten O. and Verhoeven J. *High-brightness compact X–ray source based on Cherenkov radiation. Proc. SPIE Int. Soc. Opt. Eng*, **5196**, p.393, 2004.

[11] Chefonov O., Kalinin B., Padalko D. et al. *Experimental comparizon of parametric X–ray radiation and diffracted bremsstrahlung in a pyrolytic graphite crystal. Nucl. Instr. Meth.*, B**173**, p.263, 2001.

[12] Bogomazova E., Kalinin B., Naumenko G. et al. *Diffraction of real and virtual photons in a pyrolitic graphite crystal as a source of intensive quasimonochromatic X–ray beam. Nucl. Instr. Meth.*, B**201**, p.276, 2003.

[13] Feranchuk I. and Ivashin V. *Theoretical investigation of parametric X–ray features. J. Physique*, **46**, p.1981, 1985

[14] Nasonov N. and Safronov A. *Polarization bremsstrahlung of fast charged particles. Radiation of Relativistic Electrons in Periodic Structures*, NPI Tomsk Polytechnical University, Tomsk, p.134, 1993.

[15] Knulst W. *Soft X–ray Cherenkov radiation: towards a compact narrow band source.* PhD Thesis, Technic University Eindhoven, 2004.

[16] Henke B., Gullikson E. and Davis J. *Atomic data. Nucl. Data Tables*, **54**, p.18, 1993.

[17] Nasonov N., Kaplin V., Uglov S., Piestrup M. and Gary C. *X–rays from relativistic electrons in a maltilayer structure. Phys. Rev.*, E**68**, p.03654, 2003.

[18] Nasonov N. and Safronov A. *Interference of Cherenkov and parametric radiation mechanisms of a fast charged particle. Phys. Stat. Sol.*, B**168**, p.617.

[19] Caticha A. *Transition-diffracted radiation and the Cherenkov emission of X–rays. Phys. Rev.*, A**40**, p.4322, 1989.

[20] Baryshevsky V., Grubich A. and Le Tien Hai. *Effect of multiple scattering on parametric X–radiation. JETP*, **94**, p.51, 1988.

[21] Shulga N. and Tabrizi M. *Influence of multiple scattering on the band width of parametric X–rays. JETP Lett.*, **76**, p.337, 2002.

[22] Shulga N. and Tabrizi M., *Method of functional integration in the problem of line width of parametric X–ray relativistic electron radiation in a crystal Phys. Lett.*, A**308**, p.467, 2003.

[23] Pinsker Z. *Method of functional integration in the problem of line width of parametric X–ray relativistic electron radiation in a crystal. Phys. Lett.*, A**308**, p.467, 2003.